



# Colloidal Solutions of Silicon Nanospheres toward All-Dielectric Optical Metafluids

Hinamoto, Tatsuki  
Hotta, Shinnosuke  
Sugimoto, Hiroshi  
Fujii, Minoru

---

**(Citation)**

Nano Letters, 20(10):7737-7743

**(Issue Date)**

2020

**(Resource Type)**

journal article

**(Version)**

Accepted Manuscript

**(Rights)**

This document is the Accepted Manuscript version of a Published Work that appeared in final form in Nano Letters, copyright © American Chemical Society after peer review and technical editing by the publisher. To access the final edited and published work see <https://pubs.acs.org/articlesonrequest/AOR-IW66US2Y2CEFSE8WXXQS>

**(URL)**

<https://hdl.handle.net/20.500.14094/90009538>



# Colloidal Solutions of Silicon Nanospheres toward All-Dielectric Optical Metafluids

*Tatsuki Hinamoto,<sup>†</sup> Shinnosuke Hotta,<sup>†</sup> Hiroshi Sugimoto,<sup>†,‡</sup> and Minoru Fujii<sup>\*,†</sup>*

<sup>†</sup>Department of Electrical and Electronic Engineering, Graduate School of Engineering, Kobe University, Rokkodai, Nada, Kobe 657-8501, Japan

<sup>‡</sup>JST-PRESTO, Honcho 4-1-8, Kawaguchi, Saitama 332-0012, Japan

KEYWORDS: nanophotonics, plasmonics, Mie resonance, optical magnetism, metamaterials

## ABSTRACT

A colloidal solution of nanophotonic structures exhibiting optical magnetism is dubbed a liquid-phase metamaterial or an optical metafluid. Over the decades, plasmonic nanoclusters have been explored as constituents of a metafluid. However, optical magnetism of plasmonic nanoclusters is usually much weaker than the electric responses; the highest reported intensity ratio of the magnetic-to-electric responses so far is 0.28. Here, we propose an all-dielectric metafluid composed of crystalline silicon nanospheres. First, we address the advantages of silicon as a constituent material of a metafluid among major dielectrics. Next, we experimentally demonstrate for the first time that a silicon nanosphere metafluid exhibits strong electric and magnetic dipolar Mie responses across the visible to near-infrared spectral range. The intensity ratio of the magnetic-

to-electric responses reaches unity. Finally, we discuss the perspective to achieve unnaturally high ( $> 3$ ), low, and even near-zero ( $< 1$ ) refractive index in the metafluid.

Optical magnetism is an important nature for meta-atoms constituting metamaterials. The development of dual meta-atoms which exhibit both electric and magnetic responses provides numerous opportunities for light manipulation, particularly in the field of metasurfaces, by enabling  $2\pi$  phase control<sup>1,2</sup>, Kerker-type directionality<sup>3-6</sup>, enhanced chirality<sup>7</sup>, negative refractive index<sup>8</sup>, *etc.* Although such meta-atoms are mostly lithographically defined as building blocks of solid devices, especially in the visible to near-infrared spectral range, they can also be a constituent of a liquid-phase metamaterial or a “metafluid”, if they are dispersed in solution.<sup>9-25</sup> The metafluid may find applications different from solid-state metamaterials, for example, in immersion lithography, fluidic lenses, liquid light guides, and reconfigurable optofluidic waveguide platforms for lasing<sup>26</sup>, optical switches<sup>27</sup>, and interferometers<sup>28</sup>. Over the past decades, the central interest in the metafluid research is to achieve unnaturally high, low, or even negative effective refractive indices unachievable in natural liquids.<sup>14</sup>

As a constituent of a metafluid, plasmonic nanoclusters have been primarily studied after a pioneering research on circularly assembled plasmonic nanospheres having isotropic electric and magnetic dipolar behaviors.<sup>25</sup> Various plasmonic composites including metallic nanoclusters,<sup>14,20</sup> dielectric nanoparticles decorated with metal nanospheres or nanorods,<sup>9,12,13,17,19,22,24,29</sup> and nanorod dimers<sup>18,23</sup> have been reported to realize magnetic dipolar responses in a solution. The optical magnetism of plasmonic nanoclusters relies on collective plasmonic resonances that generate circulating displacement current. Since complicated structures such as circularly assembled nanospheres are required for the generation of circulating current, the high accuracy

and high uniformity volume production is technically very challenging. In fact, because of the structural inhomogeneity, spectral features of metafluids are often broadened and washed out.<sup>13,24</sup> In particular, the magnetic responses are significantly broadened and much weaker than the electric responses. The highest measured scattering intensity ratio of magnetic dipole (MD) and electric dipole (ED) modes in a plasmonic metafluid is 0.28<sup>22</sup>, although theory often predicts much higher MD/ED ratio, *e.g.*, 1.25 for a plasmonic dodecapod.<sup>9</sup> The presence of Ohmic losses in plasmonic nanostructure and resulting heating of a solution also limits the application of plasmonic metafluids.

To circumvent these issues, we propose all-dielectric metafluids composed of high-index dielectrics as alternatives of plasmonic ones. Since dielectric nanostructures intrinsically have electric and magnetic Mie resonances, no complicated structures are necessary to realize the optical magnetism in a solution.<sup>30,31</sup> In a metafluid, the inclusions need to be smaller than the operational wavelength  $\lambda$  to treat the composite medium as an effective medium. More specifically, in the case of a dielectric nanosphere with the diameter  $D$ , the size parameter  $x = \pi D/\lambda$  should be smaller than one. Figure 1a shows the relation between the size parameter at the lowest order Mie resonance (MD:  $D \sim \lambda/n$ )  $x_{\text{MD}} \sim \pi/n$  and the refractive index  $\tilde{n} = n + i\kappa$  for different materials.  $x_{\text{MD}}$  of moderate refractive index materials such as selenium (Se), copper oxide ( $\text{Cu}_2\text{O}$ ) and titanium dioxide ( $\text{TiO}_2$ ) is larger than one, and thus they are not suitable for the inclusions of metafluids, although their colloidal suspensions are easily available.<sup>10,15,32</sup> Among the materials with  $x_{\text{MD}} < 1$ , crystalline silicon (c-Si) has almost the best balance of small  $x_{\text{MD}}$  and small loss, and thus is a promising material as inclusions of all-dielectric metafluids.<sup>9,14,33</sup> Figure 1b shows the scattering efficiency of a silicon nanosphere 150 nm in diameter in water. A distinct MD resonance is seen in addition to the ED resonance. The scattering efficiency of the MD resonance

(i.e., magnetic polarizability per unit volume) is about an order of magnitude higher than that of a plasmonic nanostructure such as plasmonic raspberry with the same size.<sup>33</sup>

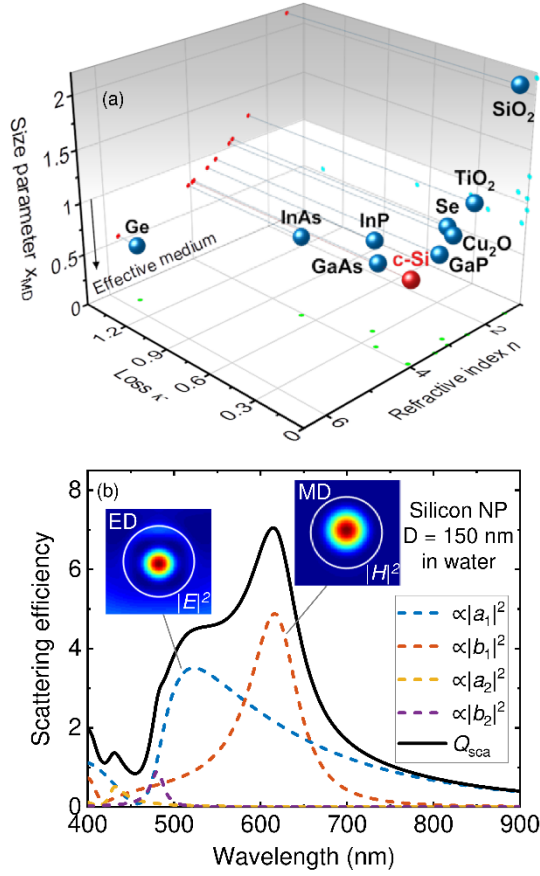


**Figure 1.** (a) Plots of size parameters at the resonant condition of the MD Mie resonance as a function of refractive index  $\tilde{n} = n + i\kappa$  of major dielectrics. The refractive indices at 600 nm are adopted. (b) Scattering efficiency (solid) and its multipolar decomposition (dashed) of a single crystalline silicon<sup>34</sup> nanosphere 150 nm in diameter in water (solid line). The contributions of the electric (ED,  $a_1$ ) and magnetic dipoles (MD,  $b_1$ ) and quadruples ( $a_2$ ,  $b_2$ ) are shown. Insets are electric and magnetic field profiles of ED and MD resonances, respectively.

In this work, we for the first time experimentally address all-dielectric metafluids made of silicon nanosphere meta-atoms operating in the visible and near-infrared spectral range. To produce high quality metafluids, silicon nanospheres should have very narrow size distributions and be dispersed perfectly in a solution, because the size distribution and the agglomeration broaden and weaken the ED and MD resonances. Recently, colloidal solutions of almost monodispersed crystalline silicon nanospheres with the diameter ranging from 90 to 200 nm have been developed.<sup>35,36</sup> Using the solutions, we show that electric and magnetic dipolar resonances can be separately observed in angle- and polarization-resolved scattering spectra. The MD/ED ratio of the solutions reaches  $\sim 1$ . Due to the difference in the resonance wavelengths between the MD and ED modes, the color of the solutions changes depending on the polarization direction of the scattered light. Following the experimental demonstration of the existence of ED and MD resonances in the silicon nanosphere metafluids, we discuss the effective permittivity, permeability, and refractive index of the metafluids and demonstrate the possibility to achieve unnaturally high, low and even near-zero refractive indices in the metafluids in the visible to near infrared range.

### **Fabrication of all-dielectric metafluids**

The fabrication procedure of colloidal solutions of silicon nanospheres is schematically shown in Figure 2a-d. The nanosphere is grown by phase separation of commercially available silicon monoxide powder into silicon and silicon dioxide by high-temperature annealing (1450°C). Silicon nanospheres are extracted from a silicon dioxide matrix by hydrofluoric acid etching and dispersed in water or in alcohol. Si nanospheres in a solution is size-separated by a density-gradient centrifugation method and almost mono-dispersed colloidal solutions are obtained. Figure 2e is a typical TEM image of size-separated nanospheres. The nanospheres are highly spherical

(circularity factor  $\sim 0.97^{36}$ ) and the crystallinity is high as can be seen in the lattice fringe in Figure 2e.

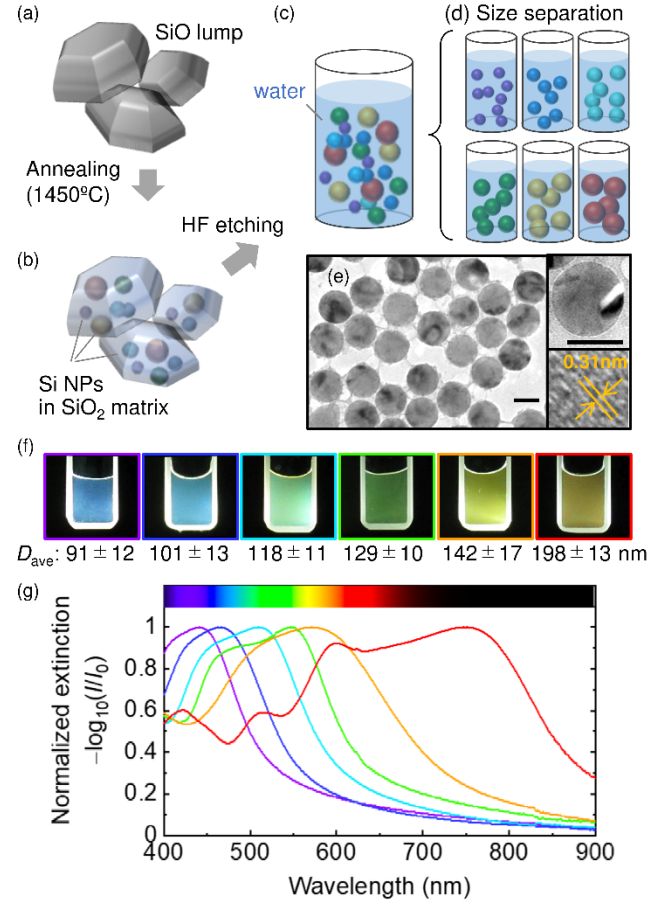


**Figure 2.** (a-d) Schematics of the fabrication procedure of colloidal silicon nanospheres. (e) TEM image of Si nanospheres (left). Enlarged image of a single nanosphere (upper right) and the high-resolution TEM image (lower right). The scale bars correspond to 100 nm. (f) Images of water solutions of silicon nanospheres with different diameters. The cuvettes are illuminated from the side and the photos are taken from the front surface. Average diameters ( $D_{ave}$ ) and the standard deviations are shown below the images. (g) Extinction spectra of the solutions in (f).

Figure 2f and g shows the photos of silicon nanosphere solutions taken under white light illumination and the extinction spectra of the corresponding solutions, respectively. The average diameters ( $D_{\text{ave}}$ ) and the standard deviations shown below the images of Figure 2f are obtained by fitting the measured extinction spectra with calculated ones (Supporting Information S1). The  $D_{\text{ave}}$  are controlled from 90 to 200 nm and the size distributions are less than 13% of the average diameters for all the samples. We can see beautiful scattering colors that change from blue to yellow with increasing the  $D_{\text{ave}}$ . The size tunability of the resonance wavelength can also be seen in the extinction spectra (Figure 2g). The wide tunability of the resonance wavelength is one of the advantages of the all-dielectric meta-atoms with respect to the plasmonic meta-atoms. In the following, we use three solutions, blue ( $D_{\text{ave}} = 101$  nm), green ( $D_{\text{ave}} = 129$  nm), and red ( $D_{\text{ave}} = 198$  nm), for the study of the properties of the metafluids. The nanosphere concentration in solutions is approximately  $10^9$  /mL. In this concentration, multiple scattering is negligible, and the Lambert-Beer law holds when the optical path length is smaller than 1 cm (Supporting Information S2).

### Light scattering by electric and magnetic dipoles in silicon nanosphere metafluid

We try to selectively measure the electric and magnetic dipolar responses of silicon nanosphere metafluids by utilizing the differences in the scattering pattern and the polarization (Figure 3a). In the Mie theory, the amplitude of  $n$ -th order electric and magnetic resonances can be obtained as Mie coefficients  $a_n$  and  $b_n$ . The azimuthal ( $\varphi$ ) and polar ( $\theta$ ) angle dependence of the scattered electric field at distance  $r$  from a sphere is

$$E_{\varphi} = \frac{\sin \varphi}{\rho} \sum_{n=1}^{\infty} E_n (b_n \xi_n \tau_n(\cos \theta) - i a_n \xi'_n \pi_n(\cos \theta)) \quad (1)$$



$$E_\theta = \frac{\cos \varphi}{\rho} \sum_{n=1}^{\infty} E_n (ia_n \xi_n' \tau_n(\cos \theta) - b_n \xi_n \pi_n(\cos \theta))$$

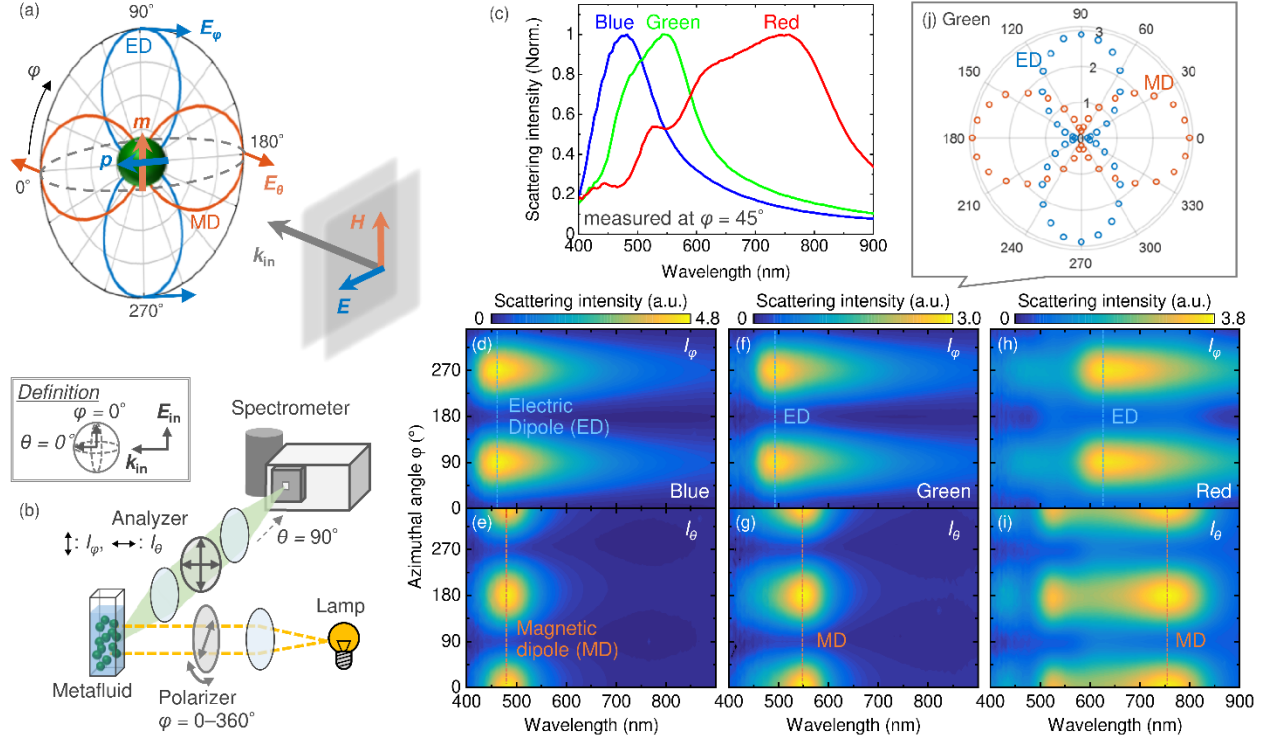
, where  $\rho = kr$ ,  $k$  is a free space wavenumber in the surrounding medium,  $E_n = i^n E_0 (2n + 1)/n(n + 1)$ ,  $\xi_n(\rho)$  is the Riccati-Bessel function,  $\pi_n = P_n^1 / \sin \theta$ , and  $\tau_n = dP_n^1 / d\theta$ .<sup>37,38</sup> In dipolar scattering,  $\pi_1 = 1$  and  $\tau_1 = \cos \theta$ . Since  $\tau_1$  vanishes at  $\theta = \pi/2$ , the dipolar electric field at  $\theta = \pi/2$  direction becomes

$$\begin{aligned} E_\varphi &= \frac{\sin \varphi}{\rho} E_1 (-ia_1 \xi_1') \\ E_\theta &= \frac{\cos \varphi}{\rho} E_1 (-b_1 \xi_1). \end{aligned} \tag{2}$$

Therefore, scattering by electric dipoles ( $a_1$ ) and magnetic dipoles ( $b_1$ ) can be separately obtained by simply measuring  $\varphi$ - and  $\theta$ - polarized scattering light, respectively, to the  $\theta = \pi/2$  direction. Note that, in the second order terms (electric and magnetic quadrupoles: EQ and MQ),  $E_\varphi = \frac{\sin \varphi}{\rho} E_2 (-3 \times b_2 \xi_2)$  and  $E_\theta = \frac{\cos \varphi}{\rho} E_2 (-3 \times ia_2 \xi_2')$ , and thus ED (MD) and MQ (EQ) have the same angular dependence. However, since the resonance wavelengths of the higher order modes are different from the dipolar modes, dipolar and higher order modes can be distinguished in the scattering spectra.

Figure 3b shows the experimental setup for the angle- and polarization-resolved scattering measurements of silicon nanosphere metafluids ( $\sim 10^9$  /mL in a  $1 \times 1$  cm<sup>2</sup> cuvette). A quartz cuvette with the light path length of 10 mm is illuminated by collimated white light from a tungsten-halogen lamp (Ocean Optics LS-1) through a polarizing prism. Light scattered to the perpendicular direction ( $\theta = 90^\circ$ ) within the half-angle of  $3.6^\circ$  is collected and led to a spectrometer equipped with a charge-coupled device (Acton Research Corporation SpectraPro-300i). An analyzer is inserted in the lens relay to separate scattering from electric and magnetic dipoles. By rotating the

polarizer ( $\varphi = 0 - 360^\circ$ ), angular distributions of scattering intensities of electric ( $I_\varphi(\varphi) \propto |E_\varphi|^2$ ) and magnetic ( $I_\theta(\varphi) \propto |E_\theta|^2$ ) dipoles are obtained.



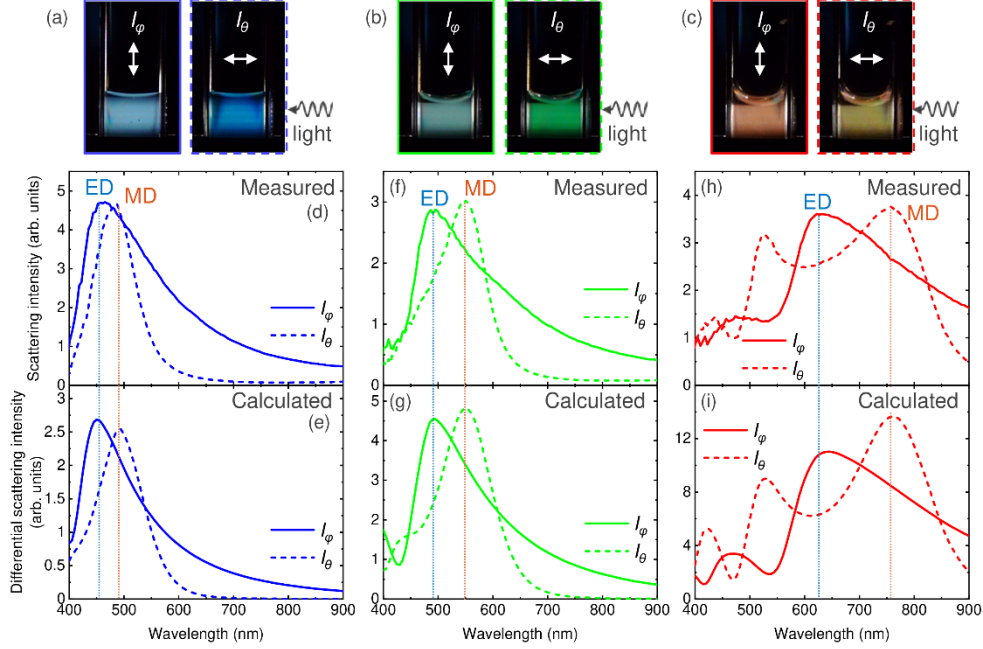
**Figure 3.** Angle- and polarization-resolved scattering spectroscopy. (a) Schematic illustration of scattering patterns and orientations of the electric fields of electric ( $p$ , blue) and magnetic ( $m$ , orange) dipoles. (b) Setup for the angle- and polarization-resolved scattering measurements. (c) Scattering spectra measured at  $\varphi = 45^\circ$  without the analyzer. Colors correspond to blue, green, and red metafluids. (d-i) Experimentally obtained scattering intensity maps of electric dipole ( $I_\varphi$ ) (d, f, h) and magnetic dipole ( $I_\theta$ ) (e, g, i) for blue (d,e), green (f,g) and red (h,i) metafluids as a function of wavelength and azimuthal angle. The blue and orange dashed lines represent scattering peaks. (j) Scattering pattern obtained by slicing the two-dimensional map of the green metafluid at the peak wavelengths of electric (495 nm) and magnetic (550 nm) dipoles.

Figure 3c shows the scattering spectra of blue, green and red metafluids measured by the setup in Figure 3b at  $\varphi = 45^\circ$  without the analyzer. Since the spectra in this configuration represent only the scattering cross sections, they are sharper than the extinction spectra in Figure 2g, which represent the sum of the scattering and absorption cross sections. Figure 3d-i shows the two-dimensional scattering maps obtained for blue (d, e), green (f, g) and red (h, i) metafluids. The ordinate is the azimuthal angle and the abscissa is the wavelength. For each metafluid, scattering intensities of electric ( $I_\varphi(\varphi)$ ) (d, f, h) and magnetic ( $I_\theta(\varphi)$ ) (e, g, i) dipoles are shown. The scattering maps of  $I_\varphi$  have peaks at  $\varphi=90^\circ$  and  $270^\circ$  with a long tail toward the longer wavelength, while those of  $I_\theta$  have peaks at  $\varphi=0^\circ$  and  $180^\circ$ . The angular dependence proves that electric and magnetic dipolar scattering have successfully been detected separately by the  $I_\varphi$  and  $I_\theta$  configurations, respectively, in Figure 3b. Figure 3j shows polar plots of  $I_\varphi(\varphi)$  and  $I_\theta(\varphi)$  of the green metafluid at the peak wavelengths, i.e., 495 and 550 nm, respectively. The plot exhibits dipolar radiation patterns which are orthogonal each other, reproducing theoretical prediction shown in Figure 3a perfectly. Similar patterns are obtained for other metafluids, 465 and 487 nm for blue, and 623 and 757 nm for red (Supporting Information S3).

The difference in the resonance wavelengths of the electric and magnetic dipoles in the metafluids can be visually recognized by the naked eye (supplementary movies are provided in the Supporting Information). Figure 4a-c shows photographs of the blue, green, and red metafluids in the  $I_\varphi(\varphi = 90^\circ)$  and  $I_\theta(\varphi = 0^\circ)$  configurations. In the  $I_\varphi(\varphi = 90^\circ)$  configuration (left), slightly whitish colors are observed due to a long tail of the electric dipole mode toward a longer wavelength, while in the  $I_\theta(\varphi = 0^\circ)$  configuration (right), highly saturated colors are observed. Figure 4d, f, h shows the scattering spectra in the  $I_\varphi(\varphi = 90^\circ)$  and  $I_\theta(\varphi = 0^\circ)$  configurations for blue, green and red metafluids, respectively. Corresponding calculated spectra are shown in Figure

4e, g, i. For the calculation, a log-normal size distribution is assumed (Supporting Information S3). We can see very good agreement between the experimental and calculated spectra. This indicates that silicon nanospheres are dispersed in the solutions without agglomeration. Most importantly, the theoretically predicted scattering intensity ratio between electric and magnetic dipole modes (MD/ED ratios) are well reproduced in the experiments. The MD/ED ratios reach 1.00, 1.05, and 1.04 for blue, green, and red metafluids, respectively. These values are more than three times larger than the highest value reported in plasmonic metafluids, *i.e.*, about 0.28 in a silver raspberry nanoparticle-dispersed metafluid.<sup>22</sup>

In the red metafluid, the spectrum in the  $I_\theta$  configuration have two peaks. In order to understand the origin of the peaks, we analyze the scattering spectra of single silicon nanospheres by the multipole decomposition. The results are summarized in the Supporting Information (S4). In the blue and green metafluids, dipolar contributions are dominant. On the other hand, in the red metafluid, the contribution of the electric and magnetic quadrupoles is not negligible below 600nm. Considering the resonance wavelength and the angular dependence, the 530 nm peak in the  $I_\theta (\varphi = 0^\circ)$  configuration in the red metafluid can be assigned to the electric quadrupole mode, while the 757 nm one to the magnetic dipole mode. Therefore, higher order resonances can also be used in the silicon nanosphere metafluid.



**Figure 4.** (a-c) Photographs and (d, f, h) measured and (e, g, i) calculated scattering spectra of the blue (a, d, e), green (b, f, g), and red (c, h, i) metafluids in the  $I_\varphi(\varphi = 90^\circ)$  and  $I_\theta(\varphi = 0^\circ)$  configurations.

### Effective refractive index of silicon nanosphere metafluid

Finally, we estimate the effective refractive index  $n_{\text{eff}}$  of silicon nanosphere metafluids. We employ the extended Maxwell-Garnett (EMG) theory, which is commonly used to calculate effective parameters of artificial composites where meta-atoms or meta-molecules are randomly dispersed (Supporting Information S5).<sup>39,40</sup> Figure 5a shows the polarizabilities of electric and magnetic dipoles of a silicon nanosphere 129 nm in diameter calculated using the Mie theory. The medium is water ( $n = 1.33$ ). The electric polarizability has a long tail toward longer wavelength, while the magnetic one exhibits almost symmetric line shape. It is worth noting that the polarizability takes a diagonal form due to the spherical shape of the inclusion and resultant

isotropic responses. By using the polarizabilities, the effective permittivity  $\epsilon_{\text{eff}}$  and the effective permeability  $\mu_{\text{eff}}$  are calculated. The results are summarized in the Supporting Information (Figure S5). In this work, we restrict our discussion in the volume fraction ( $f$ ) range below 0.5, because inclusions start to be assembled in a solution around  $f \sim 0.5$  and the EMG approach becomes inapplicable above that. The effective refractive index  $n_{\text{eff}}$  is calculated from  $\epsilon_{\text{eff}}$  and  $\mu_{\text{eff}}$  and is plotted in Figure 5b as a function of the  $f$  and the wavelength. The metafluid exhibits the effective refractive index lower than natural fluids ( $n = 1.33 - 1.55$ ) in a wide volume fraction range around 450 – 550 nm where electric and magnetic dipoles have the resonances. Even near zero index ( $n_{\text{eff}} < 1$ ) is achieved in the  $f$  region above  $\sim 0.4$ .

In order to understand the origin of the very small effective refractive index, we plot the spectra of the effective permittivity, permeability and refractive index at  $f=0.5$  in Figure 5c-e. We can see that the low  $n_{\text{eff}}$  range agrees well with the  $\mu_{\text{eff}} < 1$  range. Therefore, the magnetic dipole resonance plays an indispensable role to achieve the extremely low effective refractive index. We performed the same calculation for different size silicon nanospheres. Figure 5f shows  $n_{\text{eff}}$  as a function of the diameter of Si nanospheres and the wavelength. The volume fraction is 0.5. We can control the wavelength range of the very low refractive index by the size. We can also realize very high ( $>3$ ) refractive index in a wide wavelength range.

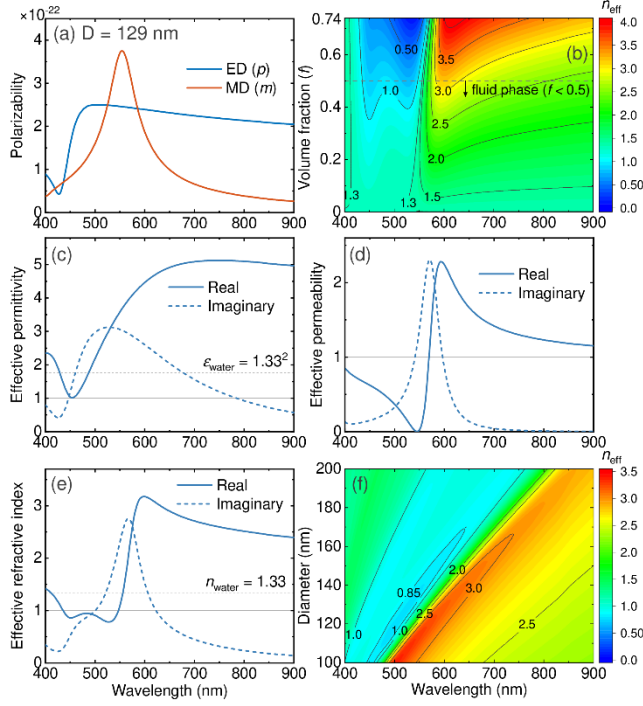


**Figure 5.** Effective refractive indices of metafluids calculated by the extended Maxwell-Garnett theory. (a) Polarizabilities of electric ( $p$ , blue line) and magnetic ( $m$ , orange line) dipoles for a 129 nm silicon nanosphere in water. (b) Effective refractive index as a function of volume fraction and wavelength. (c-e) Effective permittivity (c), permeability (d), and (e) refractive index of the metafluid. The volume fraction  $f$  is 0.5. (f) Effective refractive index as a function of nanosphere diameter and wavelength. The volume fraction  $f$  is 0.5.

## Summary

We demonstrate that a solution of size-purified silicon nanosphere exhibits strong electric and magnetic dipolar responses. The magnetic dipole response is much larger than those reported for plasmonic metafluids; the ratio of the magnetic to electric dipole responses is  $\sim 1$ . Due mainly to the strong magnetic resonance, the effective refractive index of the silicon nanosphere metafluid can be much higher and lower than natural materials, and even near-zero index ( $< 1$ ) can be

achieved around the resonance wavelengths. To the best of our knowledge, this is the first report which directly demonstrates optical magnetism of all-dielectric metafluids by macroscopic optical measurements. We believe that all-dielectric metafluids break the stagnation of the research on plasmonic metafluids arising from the structural complexity and the difficulty in the homogeneous production and open up new routes to realize tunable index fluids for optofluidic devices. Furthermore, existence of multipoles in meta-atoms provides opportunities to realize novel devices using Kerker-type multipolar interferences and helicity conservation.<sup>41</sup>

## ASSOCIATED CONTENT

**Supporting Information.** The following files are available free of charge.

Extraction of average diameters by fitting extinction spectra; silicon nanosphere concentration dependence of the extinction spectrum; scattering patterns of blue, green, and red metafluids; assignment of the scattering peaks by multipole expansion; and effective medium calculation based on the extended Maxwell-Garnett theory (PDF)

Movies exhibiting revolution of scattering colors of electric and magnetic scatterings, which correspond to Figure 4a-c (MP4)

## AUTHOR INFORMATION

### Corresponding Author

\*fujii@eedepet.kobe-u.ac.jp

## ACKNOWLEDGMENT



The authors thank Takuma Okazaki for helpful discussion and assistance in sample preparation. T. H. acknowledges the support under Grant-in-Aid for JSPS Research Fellows. H.S. acknowledges the support provided by JST, PRESTO Grant Number JPMJPR19T4. This work was partly supported by JSPS KAKENHI Grants 18J20276 and 18KK0141.

## REFERENCES

- (1) Yu, Y. F.; Zhu, A. Y.; Paniagua-Domínguez, R.; Fu, Y. H.; Luk'yanchuk, B.; Kuznetsov, A. I. High-Transmission Dielectric Metasurface with  $2\pi$  Phase Control at Visible Wavelengths. *Laser Photon. Rev.* **2015**, *9*, 412–418.
- (2) Decker, M.; Staude, I.; Falkner, M.; Dominguez, J.; Neshev, D. N.; Brener, I.; Pertsch, T.; Kivshar, Y. S. High-Efficiency Dielectric Huygens' Surfaces. *Adv. Opt. Mater.* **2015**, *3*, 813–820.
- (3) Rolly, B.; Stout, B.; Bonod, N. Boosting the Directivity of Optical Antennas with Magnetic and Electric Dipolar Resonant Particles. *Opt. Express* **2012**, *20*, 20376.
- (4) Fu, Y. H.; Kuznetsov, A. I.; Miroshnichenko, A. E.; Yu, Y. F.; Luk'yanchuk, B. Directional Visible Light Scattering by Silicon Nanoparticles. *Nat. Commun.* **2013**, *4*, 1527.
- (5) Person, S.; Jain, M.; Lapin, Z.; Sáenz, J. J.; Wicks, G.; Novotny, L. Demonstration of Zero Optical Backscattering from Single Nanoparticles. *Nano Lett.* **2013**, *13*, 1806–1809.
- (6) Geffrin, J. M.; García-Cámara, B.; Gómez-Medina, R.; Albella, P.; Froufe-Pérez, L. S.; Eyraud, C.; Litman, A.; Vaillon, R.; González, F.; Nieto-Vesperinas, M.; et al. Magnetic

- and Electric Coherence in Forward- and Back-Scattered Electromagnetic Waves by a Single Dielectric Subwavelength Sphere. *Nat. Commun.* **2012**, *3*, 1171.
- (7) Mohammadi, E.; Tsakmakidis, K. L.; Askarpour, A. N.; Dehkhoda, P.; Tavakoli, A.; Altug, H. Nanophotonic Platforms for Enhanced Chiral Sensing. *ACS Photonics* **2018**, *5*, 2669–2675.
  - (8) Atre, A. C.; García-Etxarri, A.; Alaeian, H.; Dionne, J. A. A Broadband Negative Index Metamaterial at Optical Frequencies. *Adv. Opt. Mater.* **2013**, *1*, 327–333.
  - (9) Many, V.; Dézert, R.; Duguet, E.; Baron, A.; Jangid, V.; Ponsinet, V.; Ravaine, S.; Richetti, P.; Barois, P.; Tréguer-Delapierre, M. High Optical Magnetism of Dodecahedral Plasmonic Meta-Atoms. *Nanophotonics* **2019**, *8*, 549–558.
  - (10) Cho, Y.; Huh, J.; Kim, K.; Lee, S. Scalable, Highly Uniform, and Robust Colloidal Mie Resonators for All-Dielectric Soft Meta-Optics. *Adv. Opt. Mater.* **2019**, *7*, 1801167.
  - (11) Parker, J.; Scherer, N.; Gray, S. Optical Magnetism in Core-Satellite Nanostructures Excited by Vector Beams. In *Photonic and Phononic Properties of Engineered Nanostructures VIII*; Adibi, A., Lin, S.-Y., Scherer, A., Eds.; SPIE, 2018; Vol. 1, p 53.
  - (12) Mühlig, S.; Cunningham, A.; Scheeler, S.; Pacholski, C.; Bürgi, T.; Rockstuhl, C.; Lederer, F. Self-Assembled Plasmonic Core–Shell Clusters with an Isotropic Magnetic Dipole Response in the Visible Range. *ACS Nano* **2011**, *5*, 6586–6592.
  - (13) Qian, Z.; Hastings, S. P.; Li, C.; Edward, B.; McGinn, C. K.; Engheta, N.; Fakhraei, Z.; Park, S. J. Raspberry-like Metamolecules Exhibiting Strong Magnetic Resonances. *ACS Nano* **2015**, *9*, 1263–1270.

- (14) Kim, K.; Yoo, S.; Huh, J.-H.; Park, Q.-H.; Lee, S. Limitations and Opportunities for Optical Metafluids To Achieve an Unnatural Refractive Index. *ACS Photonics* **2017**, *4*, 2298–2311.
- (15) Cho, Y.; Huh, J.-H.; Park, K. J.; Kim, K.; Lee, J.; Lee, S. Using Highly Uniform and Smooth Selenium Colloids as Low-Loss Magnetodielectric Building Blocks of Optical Metafluids. *Opt. Express* **2017**, *25*, 13822.
- (16) Urzhumov, Y. A.; Shvets, G.; Fan, J. A.; Capasso, F.; Brandl, D.; Nordlander, P. Plasmonic Nanoclusters: A Path towards Negative-Index Metafluids. *Opt. Express* **2007**, *15*, 14129.
- (17) Höller, R. P. M.; Dulle, M.; Thomä, S.; Mayer, M.; Steiner, A. M.; Förster, S.; Fery, A.; Kuttner, C.; Chanana, M. Protein-Assisted Assembly of Modular 3D Plasmonic Raspberry-like Core/Satellite Nanoclusters: Correlation of Structure and Optical Properties. *ACS Nano* **2016**, *10*, 5740–5750.
- (18) Yang, S.; Ni, X.; Yin, X.; Kante, B.; Zhang, P.; Zhu, J.; Wang, Y.; Zhang, X. Feedback-Driven Self-Assembly of Symmetry-Breaking Optical Metamaterials in Solution. *Nat. Nanotechnol.* **2014**, *9*, 1002–1006.
- (19) Sheikholeslami, S. N.; Alaeian, H.; Koh, A. L.; Dionne, J. A. A Metafluid Exhibiting Strong Optical Magnetism. *Nano Lett.* **2013**, *13*, 4137–4141.
- (20) Fontana, J.; Dressick, W. J.; Phelps, J.; Johnson, J. E.; Rendell, R. W.; Sampson, T.; Ratna, B. R.; Soto, C. M. Virus-Templated Plasmonic Nanoclusters with Icosahedral Symmetry via Directed Self-Assembly. *Small* **2014**, *10*, 3058–3063.

- (21) Vallecchi, A.; Albani, M.; Capolino, F. Collective Electric and Magnetic Plasmonic Resonances in Spherical Nanoclusters. *Opt. Express* **2011**, *19*, 2754.
- (22) Gomez-Graña, S.; Le Beulze, A.; Treguer-Delapierre, M.; Mornet, S.; Duguet, E.; Grana, E.; Cloutet, E.; Hadziioannou, G.; Leng, J.; Salmon, J.-B.; et al. Hierarchical Self-Assembly of a Bulk Metamaterial Enables Isotropic Magnetic Permeability at Optical Frequencies. *Mater. Horizons* **2016**, *3*, 596–601.
- (23) Yang, S.; Wang, Y.; Ni, X.; Zhang, X. Optical Modulation of Aqueous Metamaterial Properties at Large Scale. *Opt. Express* **2015**, *23*, 28736.
- (24) Li, C.; Lee, S.; Qian, Z.; Woods, C.; Park, S.-J.; Fakhraei, Z. Controlling Magnetic Dipole Resonance in Raspberry-like Metamolecules. *J. Phys. Chem. C* **2018**, *122*, 6808–6817.
- (25) Alù, A.; Salandrino, A.; Engheta, N. Negative Effective Permeability and Left-Handed Materials at Optical Frequencies. *Opt. Express* **2006**, *14*, 1557.
- (26) Fan, X.; Yun, S.-H. The Potential of Optofluidic Biolasers. *Nat. Methods* **2014**, *11*, 141–147.
- (27) Mansuori, M.; Zareei, G. H.; Hashemi, H. Reconfigurable Optofluidic Switch for Generation of Optical Pulse Width Modulation Based on Tunable Reflective Interface. *Appl. Opt.* **2015**, *54*, E63.
- (28) Chin, L. K.; Liu, A. Q.; Soh, Y. C.; Lim, C. S.; Lin, C. L. A Reconfigurable Optofluidic Michelson Interferometer Using Tunable Droplet Grating. *Lab Chip* **2010**, *10*, 1072.
- (29) Grillo, R.; Beutel, D.; Cataldi, U.; Rockstuhl, C.; Bürgi, T. Self-Assembled Arrays of Gold Nanorod-Decorated Dielectric Microspheres with a Magnetic Dipole Response in

- the Visible Range for Perfect Lensing and Cloaking Applications. *ACS Appl. Nano Mater.* **2020**, *3*, 6108–6117.
- (30) Evlyukhin, A. B.; Novikov, S. M.; Zywiets, U.; Eriksen, R. L.; Reinhardt, C.; Bozhevolnyi, S. I.; Chichkov, B. N. Demonstration of Magnetic Dipole Resonances of Dielectric Nanospheres in the Visible Region. *Nano Lett.* **2012**, *12*, 3749–3755.
- (31) Kuznetsov, A. I.; Miroshnichenko, A. E.; Fu, Y. H.; Zhang, J.; Luk'yanchuk, B. Magnetic Light. *Sci. Rep.* **2012**, *2*, 492.
- (32) Zhang, S.; Jiang, R.; Xie, Y.-M.; Ruan, Q.; Yang, B.; Wang, J.; Lin, H.-Q. Colloidal Moderate-Refractive-Index Cu<sub>2</sub>O Nanospheres as Visible-Region Nanoantennas with Electromagnetic Resonance and Directional Light-Scattering Properties. *Adv. Mater.* **2015**, *27*, 7432–7439.
- (33) Barois, P.; Ponsinet, V.; Baron, A.; Richetti, P. Bottom-up Production of Meta-Atoms for Optical Magnetism in Visible and NIR Light. *J. Phys. Conf. Ser.* **2018**, *963*, 012007.
- (34) Edward D. Palik. *Handbook of Optical Constants of Solids*; Academic Press: San Diego, USA, 1998.
- (35) Sugimoto, H.; Fujii, M. Colloidal Dispersion of Subquarter Micrometer Silicon Spheres for Low-Loss Antenna in Visible Regime. *Adv. Opt. Mater.* **2017**, *5*, 1700332.
- (36) Sugimoto, H.; Okazaki, T.; Fujii, M. Mie Resonator Color Inks of Monodispersed and Perfectly Spherical Crystalline Silicon Nanoparticles. *Adv. Opt. Mater.* **2020**, 2000033, 2000033.

- (37) Mie, G. Beiträge Zur Optik Trüber Medien, Speziell Kolloidaler Metallösungen. *Ann. Phys.* **1908**, 330, 377–445.
- (38) *Absorption and Scattering of Light by Small Particles*; Bohren, C. F., Huffman, D. R., Eds.; Wiley-VCH Verlag GmbH: Weinheim, Germany, 1998.
- (39) Kussow, A.-G.; Akyurtlu, A.; Semichaevsky, A.; Angkawisittpan, N. MgB<sub>2</sub>-Based Negative Refraction Index Metamaterial at Visible Frequencies: Theoretical Analysis. *Phys. Rev. B* **2007**, 76, 195123.
- (40) Ruppin, R. Evaluation of Extended Maxwell-Garnett Theories. *Opt. Commun.* **2000**, 182, 273–279.
- (41) Schmidt, M. K.; Aizpurua, J.; Zambrana-Puyalto, X.; Vidal, X.; Molina-Terriza, G.; Sáenz, J. J. Isotropically Polarized Speckle Patterns. *Phys. Rev. Lett.* **2015**, 114, 113902.

#### TOC Graphic

